Accurate Drawbead Modeling in Stamping Simulations

ACCURATE DRAWBEAD MODELING IN STAMPING SIMULATIONS

M. Sester[1], I. Burchitz[2], E. Saenz de Argandona[3], F. Estalayo[4], B. Carleer[5]

[1]AutoForm Development, Zürich, Switzerland
[2]AutoForm Engineering, Krimpen a/d IJssel, Netherlands
[3]Mondragon University, Mondragon, Spain
[4]Matrici, S. Coop, Bilbao, Spain
[5]AutoForm Engineering, Dortmund, Germany

E-mail: matthias.sester@autoform.ch

Abstract. An adaptive line bead model that continually updates according to the changing conditions during the forming process has been developed. In these calculations, the adaptive line bead's geometry is treated as a 3D object where relevant phenomena like hardening curve, yield surface, through thickness stress effects and contact description are incorporated. The effectiveness of the adaptive drawbead model will be illustrated by an industrial example.

1. Introduction

Drawbeads are frequently used in stamping tools to control the material flow. The geometrical modeling of drawbeads results in very long computation times. To overcome this problem equivalent drawbead models are applied. Stoughton proposed a model based on bending around an effective radius [1]. This model resulted in an effective description but also showed limitations. This paper describes several extensions to improve the accuracy of the equivalent drawbead model.

2. Adaptive equivalent drawbead model

2.1. Geometry and strain. The distribution of longitudinal strain depends on the sheet's bending shape. In our model, the bending shape in a partially penetrated round bead is described with five sections of constant curvature (*Figure 1*). The Stoughton model [1] employs three sections (1, 3 and 5 in our notation) with an approximated "effective radius", and two straight sections in between.

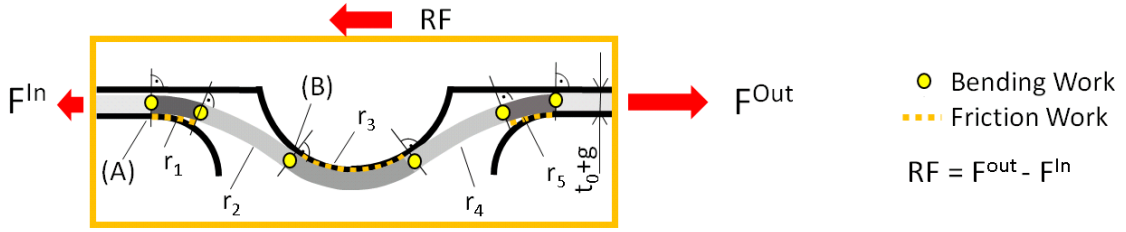

Figure 1: Bending shape with 5 sections of constant curvature $1/r_i$. Definition of restraining force RF.

The longitudinal strain change between two sections is given by the expression $\Delta\epsilon_{11} = \Delta\varepsilon_0 + \Delta\kappa\zeta$, where $\Delta\varepsilon_0$ is the mid-plane stretch increment, ζ is a natural coordinate in the sheet thickness direction, and $\Delta\kappa$ is the curvature increment $1/r_i - 1/r_{i-1}$ between current and previous section [2]. This can be interpreted as superposition of a membrane strain and a bending strain around the geometric middle.

2.2. *Material model.* An incremental elastoplastic material description defines the longitudinal stress σ_{11} from strain increments $\Delta\varepsilon_{11}$. Plasticity is modelled with Hill'48 yield condition and plane strain assumption. The equivalent plastic strain increment is given by $\Delta\varepsilon_{eq} = \frac{1+\bar{r}}{\sqrt{1+2\bar{r}}}\,\Delta\varepsilon_{11}$ with the normal anisotropy coefficient $\bar{r}$. The hardening curve $\sigma_{eq}(\varepsilon_{eq})$ relates the accumulated equivalent plastic strain $\varepsilon_{eq} = \int d\varepsilon_{eq}$ to the equivalent stress σ_{eq}. Finally, σ_{11} is computed from σ_{eq} and σ_{33} via Hill'48.

The thickness stress σ_{33} is given by a differential equation $d\sigma_{33} = (\sigma_{11} - \sigma_{33})\, dr/r$ which arises from a force balance of an infinitesimal thin layer with radius r. This equation is integrated numerically, starting at the outer surface with the natural boundary condition $\sigma_{33} = 0$. Basically, the Bauschinger effect should be essential for drawbeads due to the inherent bending/unbending [2]. We found taking into account the through thickness stress σ_{33} in the Hill48 yield surface to be more relevant than using mixed hardening.

2.3. *Section forces and section moments.* For each constant curvature section introduced above, axial forces and bending moments are evaluated from current normal stress σ_{11} and current sheet thickness t. The thinning Δt is directly determined from $\Delta\varepsilon_0$ via plastic incompressibility. The axial force is $F = \int_{-t/2}^{+t/2} \sigma_{11}\ dt$ and the bending moment is $M = \int_{-t/2}^{+t/2} \sigma_{11}\ t\ dt$. A numerical integration with N=25 integration points of equal distance is employed in our implementation.

2.4. *Thinning iteration.* The curvature change $\Delta\kappa$ is given directly by the assumed bending shape of the sheet strip, but the mid-plane stretch increment $\Delta\varepsilon_0$ and the thinning Δt are not known a priori. In our model, it follows from a procedure we call "thinning iteration". As in [2], we assume that the total curvature change $\Delta\kappa$ occurs over an infinitesimal small length along which the bending work $V_i = \int_{-\frac{t}{2}}^{+\frac{t}{2}} \left(\int_0^{\Delta\varepsilon} \sigma \Delta\varepsilon \right) dt$ is dissipated. The virtual work equation $F_{(i)} dx_{(i)} = F_{(i-1)} dx_{(i-1)} + V_{(i)}$ is used as a conditional equation for the unknown sheet thickness t and is solved iteratively. The virtual displacements $dx_{(i)}$, $dx_{(i-1)}$, the membrane strain $\Delta\varepsilon_0$ and the sheet thickness t are related via continuity and incompressibility.

2.5. *Iteration of bending shape.* In many early drawbead models, the geometry of the sheet is predetermined [1],[2],[3]. Our approach uses geometric constraints and moment equilibrium to adapt the bending form to geometry, material state and process conditions. Such an iteration of the bending shape was suggested by Sanchez and Weinmann [4]. They applied it in the framework of a finite difference scheme. We apply bending iteration to the free sections between die and bead in order to determine the unknowns r_1, r_2, r_4 and r_5 (*Figure 1*). The "entry iteration" of radius r_1 and r_2 is discussed now. Left to section 1, the sheet is straight, and right to section 2, it matches the bead. At section boundaries, normals are identical. All combinations of r_1 and r_2 that fulfil this continuity condition and do not lead to tool penetrations are called "geometric admissible states". The vertical tool gap $t_0 + g$ is crucial for the description of the bending form, as already pointed out by Yellup and Painter [3]. Among all geometric admissible solutions, the final solution is defined from balance of moments: For both sections of the unsupported region between die and bead, the moments with respect to point (A) or point (B), respectively, are evaluated. Using this reference, in the moment balance only known internal section forces and moments enter. This gives two conditions for the two unknowns r_1 and r_2 which are fulfilled by the bending iteration. In the same way, the bending form between bead radius and die *exit* radius is described.

2.6. Forces. The equivalent restraining force (RF) and equivalent uplift force (UF) are computed from the section forces and section moments defined in chapter 2.3. First, the "lever forces" $F^{Le,In}$ and $F^{Le,Out}$ between upper tool and sheet are derived (Figure 2). Lever forces are tool reactions that balance internal bending moments. They are an important element since they dominate the uplift force and contribute via frictional forces to the restraining forces. The lever force at die exit radius follows from the known section moment M of the last section and the lever arm L_e with help of a moment balance $M = F^{Le,Out} L_e$ around point (D). For the lever arm L_e a geometric assumption from a circular

segment formula is used. At the entry radius a similar relation holds.

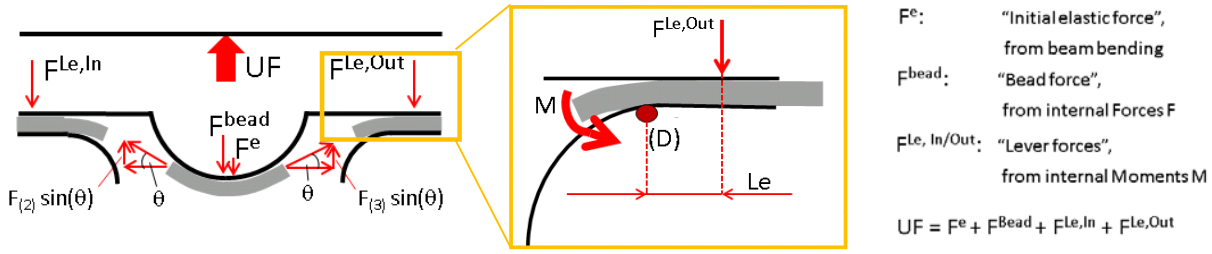

Figure 2: Definition of bead force, lever forces and total uplift force UF.

For a given bending shape, in each section the axial forces are known from the numerical solution of the virtual work equation, see chapter 2.4. The axial forces are solved section by section, and frictional forces are added where applicable. The Coulomb friction law $F^{\mu} = \mu N$ is applied for point contact, so the lever force contributes $F^{\mu} = \mu F^{Le}$. Euler's law is applied for the line contact along the bead radius, increasing F^{-} to $F^{+} = F^{-}e^{2\mu\theta}$ [1]. The equivalent restraining force is defined as the axial force increase between entry and exit, $RF = F^{Out} - F^{In}$. The vertical uplift force between sheet and the upper tool is the sum of the lever forces $F^{Le,In}$ and $F^{Le,Out}$ and the vertical part of the internal forces $F_{(2)}$ and $F_{(3)}$. For shallow beads, the initial elastic force F^{e} from elastic beam bending is added to UF, as in [1]. Finally, the uplift force $is\ UF = F^{e} + F^{Le,In} + F^{Le,Out} + F_{(2)}sin\theta + F_{(3)}sin\theta$.

2.7. *Generalization and application to double beads.* The simplest case is a single bead with no entry force applied. In general, the actual state at drawbead entry (entry force, sheet thickness, plastic strain and strain hardening) enters the model as a starting condition for the first section. This allows a straightforward application of the model to general situations, including also double beads, without additional assumptions. Note that the model nowhere does make use of fitting parameters.

2.8. Verification of uplift forces for single beads

At Mondragon University, three sheet materials and thicknesses were examined for a typical industrial round bead geometry. In Figure 3 the bead geometry is shown; measured and modelled uplift forces are plotted over bead height. The results clearly demonstrate the important role the lever forces play in our model. Without lever force, the uplift force is roughly a factor two smaller than measured. The full model reproduces the measured data well.

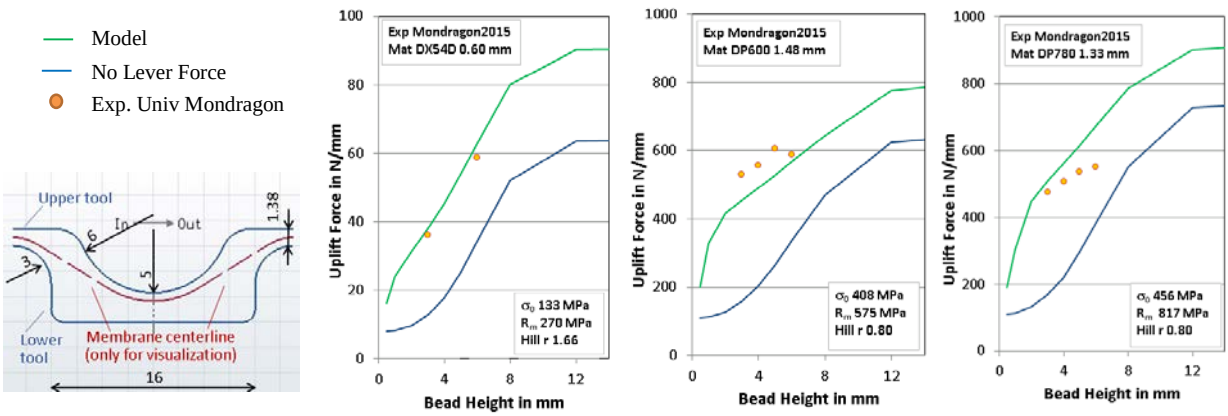

Figure 3: Example bead geometry (DP780 1.33 mm, height 5 mm). Measured uplift forces (points) by Mondragon University, modelled uplift forces (lines) with and without contribution of lever forces.

3. Application to an industrial example

Performance of the proposed equivalent drawbead model is validated using real example – underbody cross member, see Figure 4. This part was used as Numisheet 2005 benchmark, see [5].

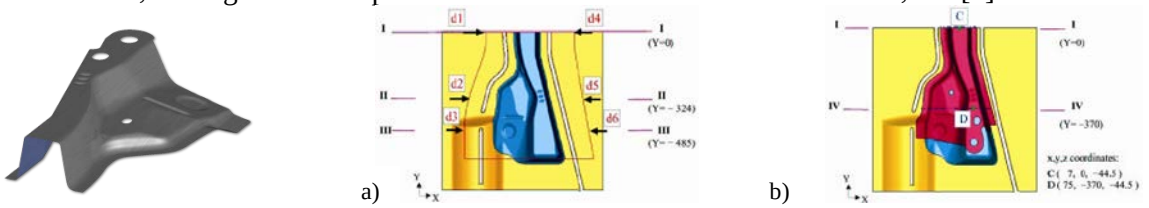

Figure 4: Underbody cross member. Sections to measure: a) draw-in; b) strains and part shape, [5].

Blank material is aluminum alloy AL5182-O. Results of two simulations are compared with real measurements. One simulation is run using the proposed adaptive line bead model and the other using geometric beads. All other process conditions as described in the conference proceedings.

Total upper die force predicted by two simulations is similar, i.e. about 1700kN. Figures 5-6 show comparison of material draw-in, true thickness strain after forming and part's shape after springback. Although results calculated with geometric beads are slightly closer to experimental measurements, adaptive line bead model gives a good prediction of typical variables used to validate a process. CPU time is about 2.5 times less compared to the geometric beads and therefore the proposed line bead model can be considered as an efficient way to incorporate drawbead effects in the simulation.

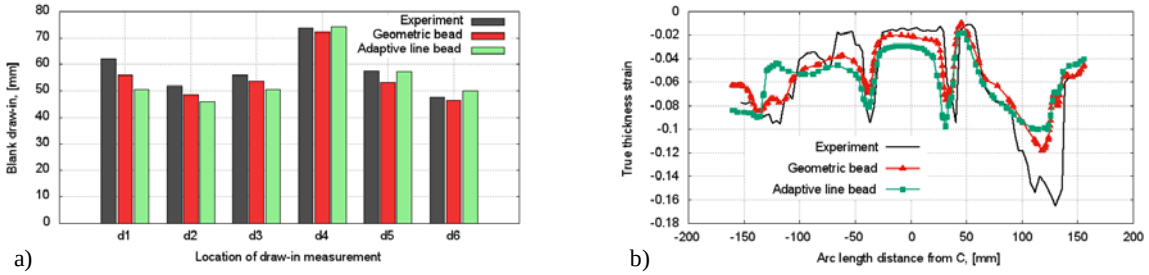

Figure 5: Simulation results: a) material draw-in after drawing; b) true thickness strain in section I

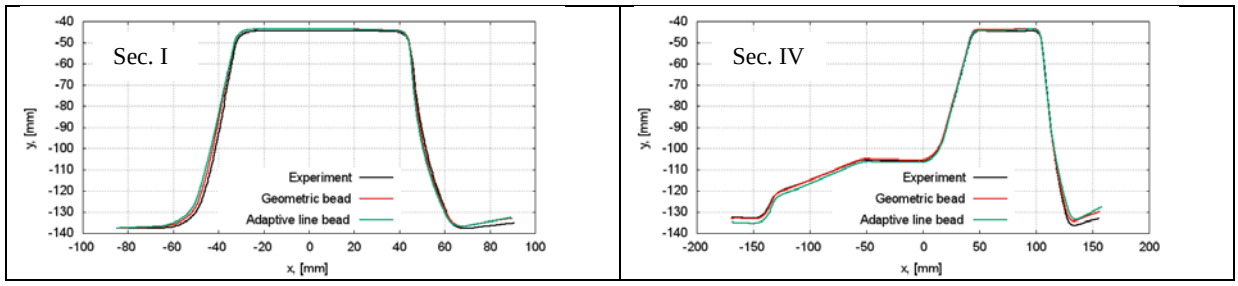

Figure 6: Springback profiles at sections I and IV.

References

[1] Stoughton T.B.: Model of drawbead forces in sheet metal forming. *Proceedings of 15th Biennal Congress of IDDRG, Dearborn, MI, 1988*

[2] Matiasson K., Bernspang L: Drawbead modelling in sheet metal stamping simulation. *Proceedings of 4th Numisheet Conference, Besancon, France, 1999*

[3] Yellup J.M., Painter M.J: The prediction of strip shape and restraining force for shallow drawbead systems. *Jounal of Applied Metalworking, Vol. 4, No. 1, pp 30-38, 1985*

[4] Sanchez L.R., Weinmann K.J.: An analytical and experimental study of the flow of sheet metal between cirular drawbeads. *Jounal of Engineering for Industry, Vol. 118, pp 45-54, 1996*

[5] L.M. Smith, F. Pourboghrat, J.W. Yoon, and T.B. Stoughton, editors. *Proc. of 6th Numisheet Conf.*, Detroit, MI, 2005